J. Fluid Mech. (1983), *vol.* 135, *pp.* 123–153
Printed in Great Britain

Turbulent boundary-layer flow and structure on a convex wall and its redevelopment on a flat wall

By J. C. GILLIS
S. Levy Inc., 1999 S. Bascom Avenue, Campbell, CA 95008

AND J. P. JOHNSTON
Department of Mechanical Engineering, Stanford University, CA 94305

Two experiments ($\delta/R = 0.05$ and 0.10) were performed to determine how boundary-layer turbulence is affected by strong convex curvature. The flow passed from a flat surface, over convex surface with 90° of turning, and then onto a flat recovery surface. The pressure gradient along the test surface was forced to be zero.

After the sudden introduction of curvature, the shear stress in the outer part of the boundary layer is sharply diminished. The wall shear also drops off quickly downstream. When the surface suddenly becomes flat again, the wall-shear and the shear-stress profiles recover very slowly towards flat-wall conditions. The shear-stress profiles in the curved region for both experiments collapse when $-\overline{uv}/u_\tau^2$ is plotted *vs.* distance from the wall normalized on wall radius, n/R. The strong-curvature data of So & Mellor also fall on the same curve. Thus suggests an asymptotic state for the shear-stress profiles of strongly curved boundary layers where R rather than boundary-layer thickness controls the active turbulence lengthscales. In this asymptotic region, the active shear-layer thickness is less than its initial value at the start of curvature. In the recovery region, the width of the active shear layer regrows slowly within the original velocity-gradient boundary layer, like a developing boundary layer under a free stream with a velocity gradient normal to the wall.

1. Introduction

Ever since Bradshaw's (1969) paper on the effects of streamline curvature on turbulence, everincreasing attention has been paid to the effects of extra strain rates. This paper presents results of two new experiments where flat-plate boundary layers were subjected to sustained convex longitudinal curvature and subsequently allowed to recover on a flat surface.

The first investigations of the effects of curvature on turbulent shear flow were undertaken by Ludwig Prandtl soon after he laid the foundations of boundary-layer theory. His students, Wilcken, Wendt, Wattendorf and Schmidbauer carried out mean-velocity measurements in various curved duct flows. From these mean measurements, the magnitude of the turbulent shear stresses were deduced and the effective mixing lengths were calculated. These results showed a great reduction in the apparent lengthscale of the turbulence when the shear-layer flows over a convex wall.

Prandtl recognized that this reduction in scale could be tied to a simple stability argument based on consideration of an inviscid flow, proposed by von Kármán (1934). Von Kármán's argument, as quoted by Bradshaw (1973), was that, in an inviscid irrotational flow with convex curvature, velocity decreases in the direction away from

the centre of curvature. If a fluid element travelling in a circular path in equilibrium is displaced a small distance away from the centre of curvature, a simple balance of forces on that element shows that the radial pressure gradient at its new location is slightly larger than what is necessary to move it in a circular path. The element is then forced back towards the centre of curvature. Conversely, if an element is displaced towards the centre of curvature, the pressure gradient at its new location is not strong enough to bend the element's path around the tighter radius of curvature and it will move back out towards its original equilibrium position. In an inviscid, irrotational flow with convex curvature, then, there is a natural tendency for fluid elements to stay close to the particular streamline where their velocity is matched to the local radial pressure gradient.

A similar conclusion was reached by Rayleigh (1917) about inviscid flows with circulation. In the case of simple circular flows where velocity is a function only of the radius of curvature R, the flow is unstable to small displacements when the derivative $\mathrm{d}\Gamma/\mathrm{d}R$ of circulation with respect to R is less than zero. If $\mathrm{d}\Gamma/\mathrm{d}R$ is greater than zero, the flow is stable – small displacements perpendicular to streamlines are damped out. The former condition corresponds to boundary-layer flow over a concave wall and the latter (stable) condition corresponds to flow over a convex wall.

Even though inviscid arguments do not apply strictly to turbulent flow over a convex surface, the arguments do imply that the flight of a fluid element that is displaced normal to a stably curved mean streamline by a velocity fluctuation will be shorter than in a plane flow. The effect of this damping on the turbulence would be to confine the effect of any turbulent event closer to the originating radial position than in a flat-wall flow. One might then expect that the largest eddies in flow over convex surfaces would be smaller than for a corresponding flow over a flat surface. This argument cannot be made quantitative, because it comes from purely inviscid considerations. However, it is supported by the data of Eskinazi & Yeh, which will be further discussed later.

The first experiments on flow over convex surfaces were done by Prandtl and his students at Göttingen. Prandtl had apparently convinced himself from mixing-length arguments that the stabilizing effect just described would have only negligible effect on convex boundary-layer turbulence. He decided that the effects of curvature, both concave and convex, could be predicted by including in his mixing-length model a curvature parameter as

$$l = l_0\left[1 - \frac{1}{4}\frac{U/R}{\partial U/\partial n}\right].$$

(In this paper, s will denote distance parallel to the wall, n will denote distance normal to the wall.) This was the first in the series of schemes which have been tried to model curvature effects accurately. However, the experimental results of Prandtl's student Wilcken showed that the mixing length in a convexly curved boundary layer (back-calculated from the mean-velocity profiles) was much less than predicted by Prandtl's theory and greatly reduced from its flat-wall value. Further work by other students confirmed these results (Wendt 1933; Wattendorf 1935; Schmidbauer 1936. The general conclusion – that, even for small values of δ/R, the boundary-layer hydrodynamics are greatly affected – was published, but this strange result did not inspire further published investigations.

Note that the ratio of layer thickness δ to wall radius of curvature R is the accepted parameter describing the magnitude of the curvature effects on the outer layer of the

flow. For $\delta/R \lesssim 0.01$, these effects are generally weak to moderate; but for $\delta/R \gtrsim 0.1$ they are overwhelming, and, as we shall see, this parameter ceases to have practical meaning.

In the mid-1950s experiments were conducted in a curved-channel flow by Eskinazi & Yeh (1956). Using hot-wire anemometry, a fairly new technique at that time, they took the first measurements of turbulence quantities and drew important conclusions. Their experiments showed a great decline in values of $(\overline{u'^2})^{\frac{1}{2}}$ and $(\overline{v'^2})^{\frac{1}{2}}$ over the convex surface, and their spectral measurements showed that the decline was largest in the low-wavenumber (large-wavelength) range. The fact that the wavelength decline was largest in the low-wavenumber range supports the idea advanced earlier, that the damping effect of the radial pressure gradient reduces the size of the largest eddies. They related this drop qualitatively to the effects of curvature on the production term in the Reynolds stress transport equations.

Interest in the effects of curvature intensified in the late 1960s, possibly because, by this time, calculational models had been developed to the point where the effects of curvature were not lost in other inaccuracies. One of the first published experiments of this era was performed by Patel (1968) in a wind tunnel with a 90° bend. He measured only mean quantities, and these measurements may have been influenced by secondary flows on the tunnel's endwalls. Nevertheless, he was able to come to the correct conclusion that curvature affects entrainment by examining the variation of the shape factor, δ_1/δ_2.

At about the same time as Patel's work, Thomann (1967) published a set of experiments on heat transfer in curved boundary layers. They proved that the Stanton number is affected in much the same way as the skin friction, but no measurements of the hydrodynamic boundary layer were taken. Thomann's measurements were also noteworthy in that they were the first to be performed at supersonic free-stream Mach number.

In 1972, So & Mellor published results from a very detailed experiment on a curved-wall boundary layer. In this experiment the ratio of boundary-layer thickness to radius of curvature was large enough that several gross effects were demonstrated. All the Reynolds stresses were measured, and the flow was acceptably two-dimensional wall. On the convex wall it was found that the turbulent shear stress was 'turned off' (the value of $\overline{u'v'}$ was approximately zero) in the outer half of the boundary layer.

Wall shear stress was inferred from a Clauser plot, but the turbulent shear stress profile was not measured close enough to the wall to check all values by extrapolation. The accuracy of the shear stress measurements very near the wall has been questioned lately by So (1978).

Over the concave wall, they found evidence of a system of streamwise axial vortices, analogous to those found between rotating cylinders. These vortices were strong enough to make the mean flow inherently three-dimensional. Concave flows with their three-dimensional phenomena will not be further considered in this paper.

In 1969, Bradshaw pointed out the analogy between the effects of curvature and the effects of buoyancy. He then proposed that the Monin–Oboukhov formula for the correlation of the apparent mixing length with small buoyancy effects

$$\frac{l}{l_0} = 1 - \beta Ri$$

(where β is a positive empirical constant and Ri is the Richardson number) could be

used to model the effects of weak curvature if the 'curvature Richardson number' was defined as

$$Ri_c = \frac{2U/R}{\partial U/\partial n}.$$

This approach met with considerable success. In fact, the value of the constant β could be inferred by analogy from meteorological experiments in stably and unstably stratified boundary layers, where it was found to be of the order of 10. This model was used by numerous workers, such as Johnston & Eide (1976), Rastogi & Whitelaw (1971) and Cebeci, Hirsh & Whitelaw (1978), each with slight modifications.

In the 1970s the pace of work on curvature increased greatly. Bradshaw undertook a series of experiments on the effects of very weak curvature ($\delta/R \approx 0.01$), working first with Meroney (1975) and later with Hoffmann (1978). Despite the fact that the curvature was much less than for So & Mellor, there was a noticeable decline in the shear-stress levels in the outer region. The outer-layer mixing-length values declined slowly as the flow moved downstream of the start of convex curvature; eventually the values were about one-half of their corresponding flat-wall values. A similar experiment was performed by Ramaprian & Shivaprasad (1978).

Simultaneously with the work described above, Castro & Bradshaw (1976) were characterizing a highly (convex) curved mixing layer. This was the first experiment to examine the recovery process, that is, how the effects of curvature die away after a longitudinally curved shear-layer flow becomes straight again. In the early stages of recovery, their data showed an 'overshoot' in value of the turbulent kinetic energy relative to its equilibrium plane-layer value.

The first direct measurements of the recovery process in boundary layers were taken by Smits, Young & Bradshaw (1979) at Imperial College. Their flow was set up to show the effects of an 'impulse of curvature' in which a normal flat-plate boundary layer was subjected to extremely strong curvature ($\delta/R \approx 0.2$) through a short turning angle (20° or 30°). Their results showed the recovery to be a slow and non-monotonic process. No measurements were taken within the short bend. However, some of their results are similar to the observations reported here.

In recent years, models much more complicated than simple mixing-length models have been used to predict turbulent flows. Not surprisingly the models for curvature effects have also become more complicated. Multi-equation models based on the work of Launder, Reese & Rodi (1975) have been proposed by Irwin & Smith (1975), whose model modified the Launder, Reese & Rodi model by including the extra Reynolds stress production terms which appear naturally in those equations. The work of Gibson, Jones & Younis (1980) differed from that of Irwin & Smith in details of the pressure-strain modelling. Launder, Priddin & Sharma (1977) applied the empirical concepts of Bradshaw to the two-equation turbulence model of Jones & Launder (1972).

Even though the number of data sets that show the effects of convex curvature has grown in the last 10 years, our understanding of the physical processes is still relatively poor and the development of really good calculational models is being held back by a lack of reliable data. In § 2 of this paper, results of a new set of experiments will be presented, which will provide a little more information about how a boundary-layer flow responds to convex curvature and how it recovers from strong convex curvature.

In the experiment to be described, careful measurements were taken to show the response of the boundary layer to a sudden change from flat wall to curvature, and later from curvature to flat wall. It was found, to our surprise at first, that, although

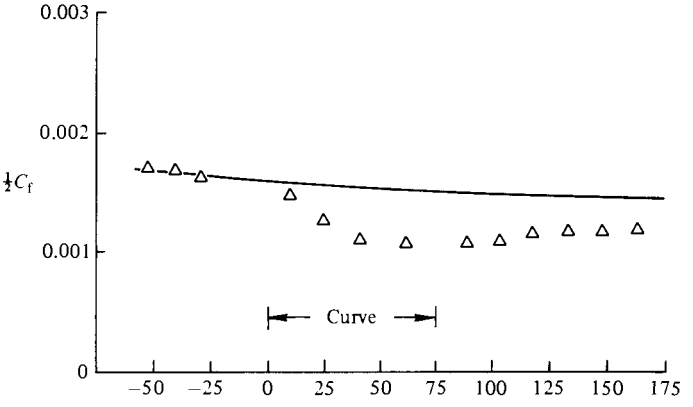

FIGURE 1. Skin friction *vs.* distance in flow direction: △, experiment; ——, flat-wall prediction (STAN5).

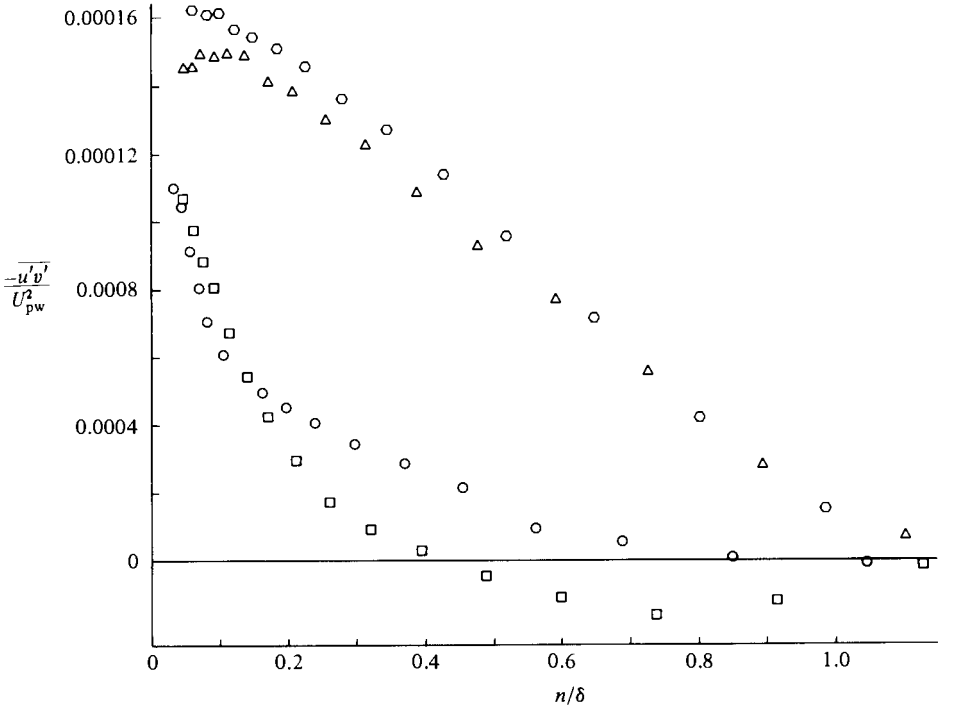

FIGURE 2. Shear-stress profiles near the start of curvature: ○, flat-wall upstream of curvature; △, exactly at the start of curvature; ○, after 13° of curvature; □, after 30° of curvature.

curvature effects were clearly apparent one or two boundary-layer thicknesses downstream of the start of curvature, the disappearance of those curvature effects on a flat wall was an extremely slow process. This asymmetrical behaviour is illustrated by figures 1 and 2, which show the skin-friction distribution over the whole test surface, and the shear-stress profiles close to the start of curvature.

After some contemplation, it is clear that this asymmetric behaviour, and other results of the experiments of §2 follow, or are consistent with, the argument previously stated, that the radial pressure gradient should act to reduce the size of

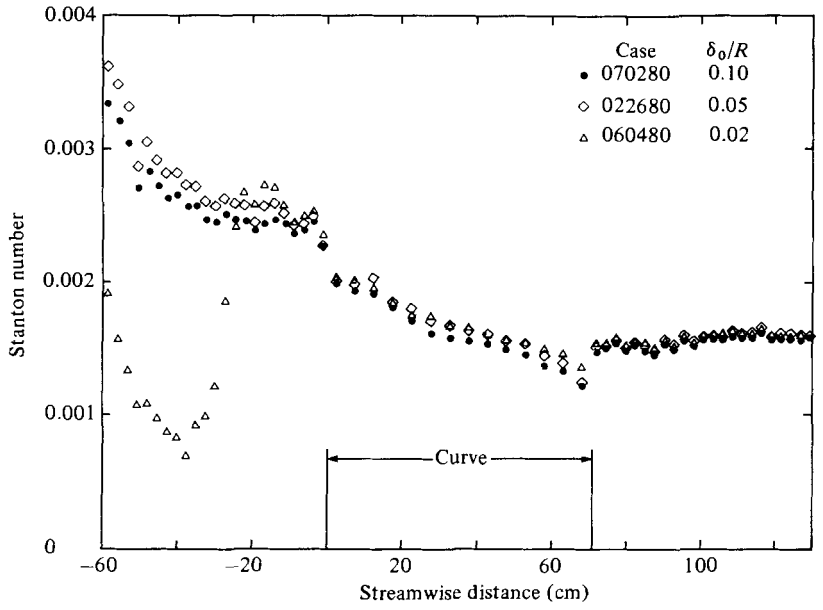

FIGURE 3. The effect of initial boundary-layer thickness on heat transfer (data of Simon 1980): ●, $\delta/R = 0.10$; ◇, 0.05; △, 0.02.

the largest eddies. This reduction is quite obvious in figure 2, in which the width of the region where the u' and v' fluctuations have significant correlation has been reduced from over δ to under $\frac{1}{3}\delta$.

Such a reduction in scale means that the large-scale eddies, which contain information from upstream – the 'history' of the turbulence structure – must either shrink or disappear. If the reduction in scale is large enough and occurs fast enough, then the influence of upstream conditions on the turbulence structure will be less, and a local parameter, the radius of curvature, will be very important in determining the turbulence structure. This is not to say that all influence of upstream conditions is lost – clearly the mean velocity field is a product of upstream conditions, but one will expect the turbulence structure of dissimilar boundary layers to become similar after the onset of strong curvature.

The data of the experiments to be described support this argument. In figure 3 we have the heat-transfer data of Simon (1980), which show Stanton number as a function of streamwise distance, for three boundary layers, whose Reynolds numbers at the start of curvature vary by a factor of *five*. Downstream of the start of curvature, the Stanton numbers are extremely close. A similar result is shown in figure 4, where shear-stress measurements from four convex-wall experiments (So & Mellor 1972; Gillis & Johnston 1980; and two to be described) are plotted together *vs.* distance from the wall divided by radius of curvature. The profiles fall on top of each other, indicating the importance of the radius of curvature as a scaling parameter of the turbulence structure, at least when $\delta/R > 0.05$ and the effect is strong.

Finally, the slow recovery from curvature effects, shown by the skin-friction and heat-transfer coefficients of figures 1 and 3, is also consistent with the idea that the stabilizing effect of convex curvature acts to reduce permanently the turbulence lengthscale and lessen the effects of the upstream conditions. At the end of curvature, the turbulence structure does not spring back to its original state as if it had been

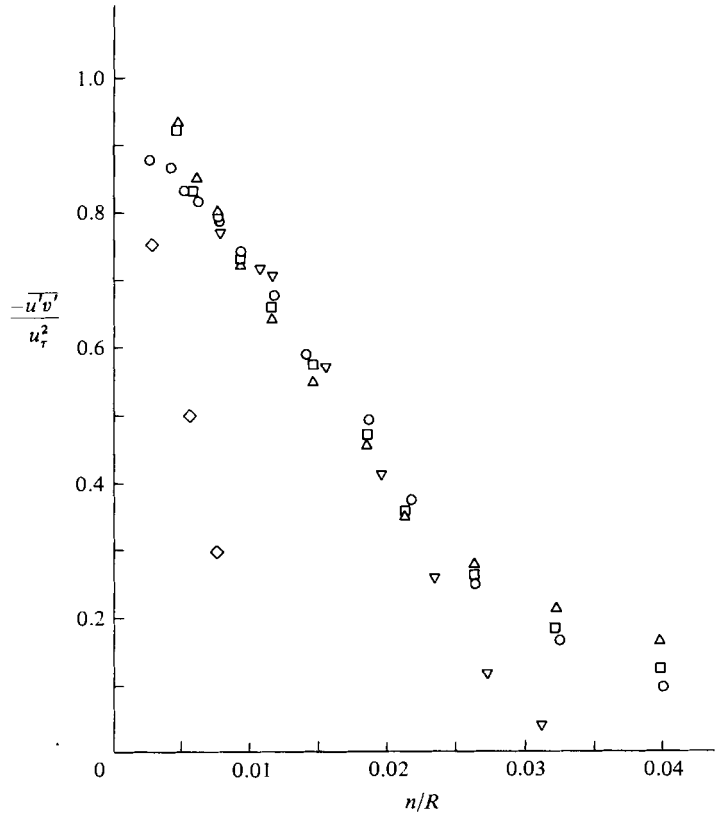

FIGURE 4. Collapse of shear-stress profiles from several experiments, all taken after sustained curvature: ▽, So & Mellor (1972); ○, Gillis & Johnston (1980); □, present results, $\delta/R = 0.10$; △, present results $\delta/R = 0.05$; ◇, Hoffman & Bradshaw (1980), $\delta/R = 0.01$.

artificially held down in the curve. Instead, the turbulent eddy structure must slowly enlarge itself in the same way that the turbulence structure of a developing flat-plate boundary layer enlarges itself. Therefore the slow recovery might have been expected had we thought more carefully in the first instance.

2. Experiments on convex curvature

A series of experiments was undertaken to gather more data on the effects of convex curvature. The experiments were similar to the convex side of the So & Mellor experiment, but in this case they were designed to allow study of the onset of curvature and, particularly, how curvature effects disappear downstream of curvature. In the layout used, a two-dimensional turbulent boundary layer passes over a flat development surface onto a convex curved surface and then back onto a flat (recovery) surface. As in the previous experiment of Gillis & Johnston (1980), careful contouring of the concave side of the tunnel allowed us to control static pressure so that the pressure coefficient

$$C_p = \frac{P_{\text{wall}} - P_{\text{wall},\,s=0}}{\frac{1}{2}U_{\text{pw}}^2},$$

varied but never had an absolute value greater than 0.027. The experiments were also designed to allow data to be taken with different values of δ_0 (the boundary-layer

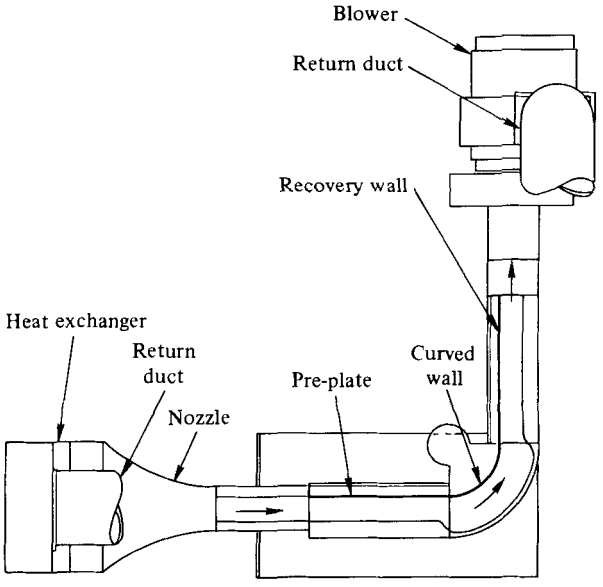

FIGURE 5. Plan view of the experimental facility.

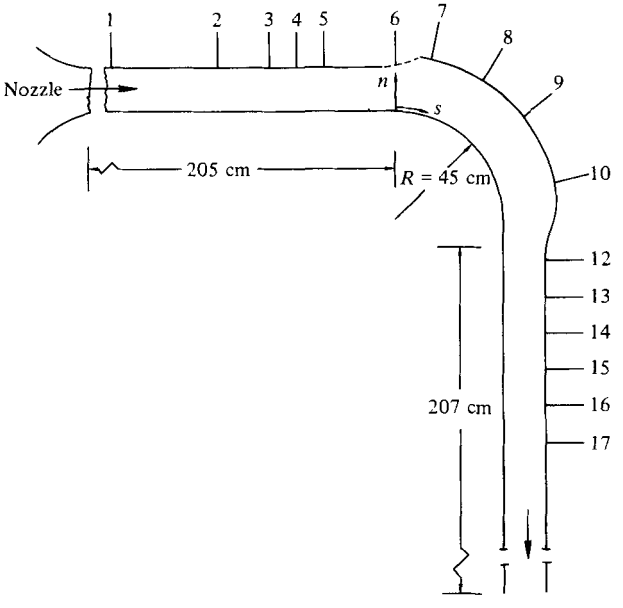

FIGURE 6. Measurement stations.

thickness at the start of curvature), because it was originally thought that the ratio of δ_0 to the radius of curvature would be the parameter controlling the effects of curvature and the downstream behaviour of the boundary layer. As figure 4, based on several data sets, shows, however, δ_0/R has very little, if any, influence for values larger than 0.05. Two major data sets are presented here for values of $\delta_0/R \approx 0.10$, close to the results reported by Gillis & Johnston (1980) and for $\delta_0/R \approx 0.05$. The larger δ_0/R results are presented first (see figures 1, 2 and 7–15).

Experiments on convex surfaces which form one wall of a rectangular duct are always complicated by the secondary flows, which are driven down the sidewalls by the radial pressure gradient and which then flow out into the boundary layer on the test surface. This was particularly true in this experiment, in which two-dimensionality had to be maintained not only through the curved section but also in the long recovery section. It will be shown that we were successful in controlling these secondary flows.

Figure 5 shows a layout of the wind tunnel and related equipment. Although similar in design to the original apparatus of Gillis & Johnston (1980), this test facility is completely new. The primary differences are improved secondary-flow control and a recovery section that is twice as long as that in the earlier rig. The blower is mounted at the end of the test section; it moves air through a return duct to a plenum. Downstream of the plenum, the flow passes through a heat exchanger, a flow straightener and six sets of screens. The flow is then accelerated through a two-dimensional nozzle with an 11 : 1 area ratio. Following the contraction, the potential core has a velocity profile flat within 0.15 percent of the mean and a streamwise turbulence intensity

$$(\overline{u'^2})^{\frac{1}{2}}/U_{\mathrm{pw}}$$

about equal to 0.5 %.† After being tripped just downstream of the nozzle exit, the boundary layer was allowed to develop over a flat preplate 205 cm long. The test surface then had a 90° bend of 45 cm radius, before flowing over the 205 cm long recovery plate. The test surface was 127 cm wide and, at the nozzle exit, the tunnel height (normal to test surface) was 50 cm. Figure 6 shows the stations where measurements were taken.

Mean velocity measurements were taken from wall static pressure taps and Pitot tubes which were traversed across the boundary layer (n-direction). In the curved region, the static pressure P_{sw} was read at the wall, and the local velocity was then calculated from

$$U = \frac{2}{\rho}(P_{\mathrm{t}} - P_{\mathrm{sw}}) - (P_{\mathrm{r}} - P_{\mathrm{sw}})\left[1 - \frac{1}{(1+n/R)^2}\right],$$

where P_{t} is local total pressure and P_{r} is free-stream total pressure. The equation is derived and explained by Gillis *et al.* (1980).

Mean-velocity measurements were also taken using a DISA 55M01 constant-temperature anemometer, a TSI 1076 linearizer and a DISA 55P01 horizontal-wire probe. Because of the limitations of hot wires, these mean-velocity measurements are less accurate than the Pitot-probe data. However, they were useful to check the Pitot data, and, at the station at the start of curvature (where the wall static-pressure distribution was unknown). they provided the only mean measurements.

The horizontal-wire's bridge signal was used in conjunction with a TSI 1076 linearizer and a DISA 55D35 true r.m.s. meter to measure turbulence intensities. Measurements of the Reynolds stress tensor were made using two DISA 55M01 bridges, two TSI 1076 linearizers, and a DISA 55P51 X-wire probe. Details are given by Gillis *et al.* (1980).

† In this experiment the velocity U_{p} of the potential flow is not constant, but a function of local radius of curvature. The reference velocity U_{pw} is the potential velocity at the wall, which is related to U_{p} by $U_{\mathrm{p}} = U_{\mathrm{pw}}(R/(R+n))$ This definition differs slightly from the definition used by some workers of $U_{\mathrm{p}} = U_{\mathrm{pw}}\mathrm{e}^{-y/r}$. The difference for a flow where $\delta/R \approx 0.10$ is a maximum of less than 0.5 %.

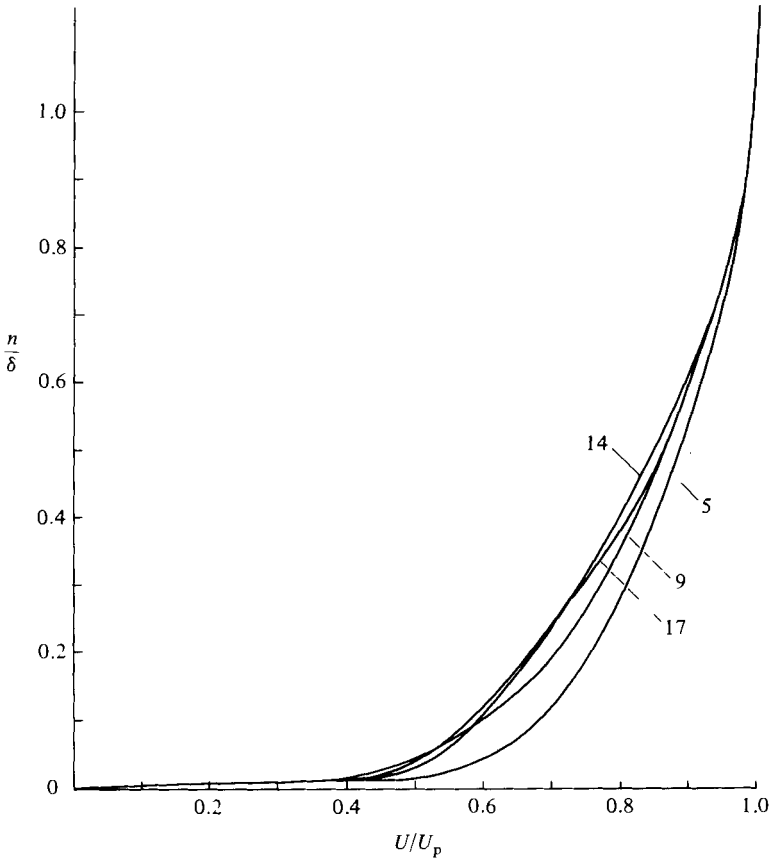

FIGURE 7. Mean-velocity profiles for four representative stations, $\delta/R = 0.10$ (see figure 6 for station definitions).

2.1. *Mean-velocity profiles*

Figure 7 shows four mean-velocity profiles taken at four representative stations: one upstream of curvature (5), one in the curve (9), and two in the recovery section (14 and 17). The boundary-layer width used in figure 7 and throughout this paper is the 99% thickness. The abscissa in figure 7 is the local velocity normalized on U_p, the potential-flow velocity using the local radius of curvature. The upstream profile compares well with that expected for a fully turbulent boundary layer; the momentum-thickness Reynolds number $U_{pw}\delta_2/\nu$ is 3378 and the shape factor H is 1.32. The profile (9) after 53° of bend, however, looks more like a transitional or even a laminar boundary layer. The velocity gradient is higher in the wake region, and, although it is not readily apparent from figure 7, the velocity gradient is lower near the wall. Originally, it was expected that in the recovery region the velocity profiles would relax back toward the upstream profile as the flow moved downstream in the recovery region. However, the velocity gradient in the outer part of the layer ($n/\delta > 0.4$) continues to increase to the end of the recovery region, and the shape factors also remain high. At the last station (17) in the recovery region, there does seem to be some recovery taking place very close to the wall, below $n/\delta = 0.05$.

The fact that the values of U/U_p along a given streamline (or approximately at given n/δ) is *increasing* as the flow moves downstream in the recovery region permits

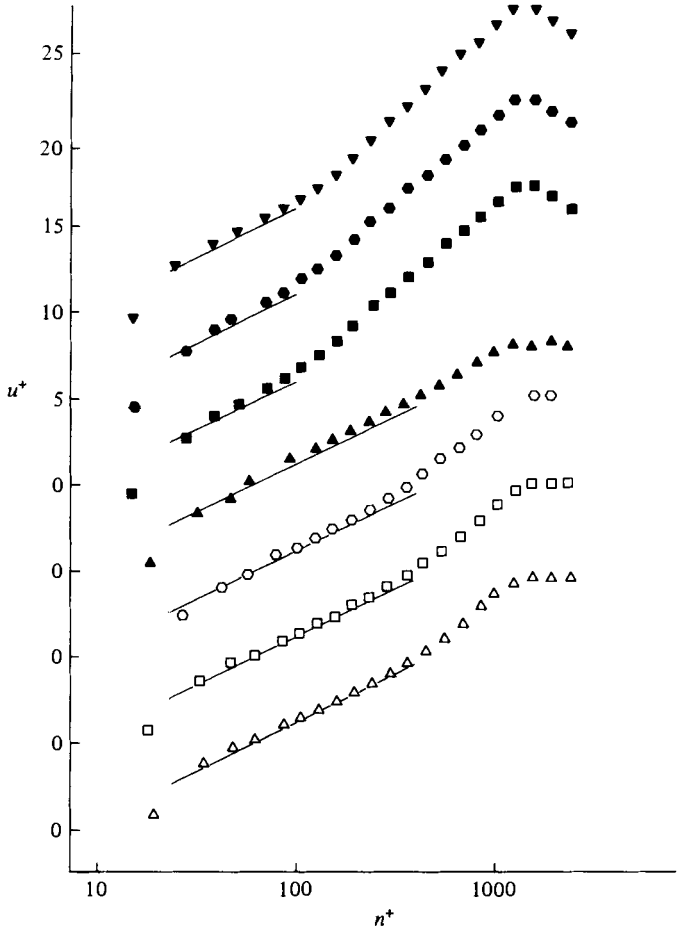

FIGURE 8. Non-dimensional mean-velocity profiles plotted on semilog paper: △, station 3; □, 4; ○, 5; ▲, 7; ■, 8; ●, 9; ▼, 10. Note closed symbols for curved flow. Lines are $u^+ = 2.44 \ln y^+ + 5.0$.

certain inferences to be drawn about the shape of the shear-stress profile. As pointed out by Smits *et al.* (1979), the momentum equation along a streamline reduces to

$$\frac{\partial P_t}{\partial s} = \frac{\partial \tau}{\partial n},$$

where P_t is the stagnation pressure and τ is the total shear stress. For the recovery region points, very near the wall, P_t is increasing downstream. Since τ drops to zero at the edge of the boundary layer, one concludes that the gradient of τ must be positive near the wall and that it must reach a maximum *away from the wall*, even when the streamwise static pressure gradient is zero, $\partial P_s/\partial s = 0$, as it is near the wall.

Figure 8 shows the profiles plotted in inner coordinates. As has been noted before by So & Mellor (1972) and Ramaprian & Shivaprasad (1978), the profiles in the curved region follow the law of the wall, although they become non-logarithmic at a lower value of n^+. There appears to be a *second* logarithmic zone from $n^+ \approx 200$ to $n^+ \approx 1500$, a fact not noted previously.

The fact that the log law is valid over less of a region than for a flat wall may be

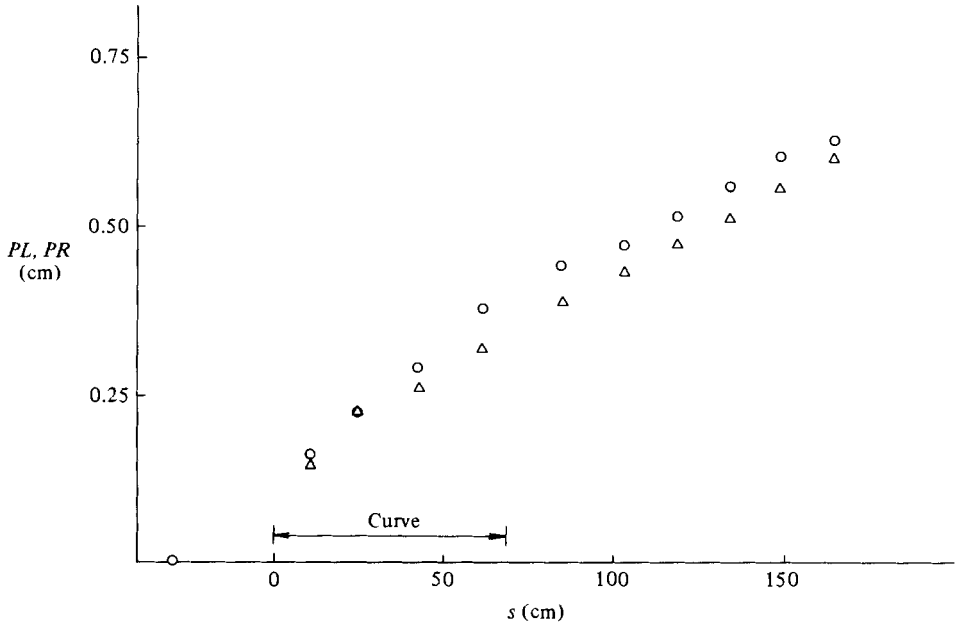

FIGURE 9. PL and PR for experiment at $\delta/R = 0.10$: ○, PL (the integrated momentum deficit); △, PR (the integrated skin friction).

due to the fact that, for a curved wall, u is a function of three dimensionless groups:

$$\frac{u}{u_\tau} = f\left(\frac{nu_\tau}{\nu}, \frac{n}{R}, \frac{n}{\delta}\right).$$

If R is small enough, then only nu_τ/ν is important, and the classical log law holds. If R is large enough, then the mean velocity in the wake will be a function of n/δ. However, if R is small, then the breakdown of the overlap region where the log law holds will be due to the dominance of the function of n/R, while n/δ is still small.

The skin-friction coefficient $\frac{1}{2}C_f$ was computed by the Clauser-plot method; results have already been shown plotted in figure 1. As discussed earlier, the skin friction is still far below its flat-wall value at the end of the recovery section, a distance cf about 15 boundary-layer thicknesses from the end of curvature. The data of Smits *et al.* (1979) show that C_f does begin to approach its flat-wall value, but only after about 50 boundary-layer thicknesses.

From the mean-flow measurements, it was possible to check the two-dimensionality of the flow by comparing, at each station, the measured momentum thickness PL to the momentum thickness calculated from the momentum integral equation and the measured skin friction PR.

In the curved region, the form of the momentum integral equation used was that devised by Simon & Honami (1980). The formulas they arrived at were

$$PL = \frac{1}{(\delta_{2m} U_{pw}^2)} \delta_{2m} U_{pw}^2 - [\delta_{2m} U_{pw}^2]_{s_0} P + \int_{s_0}^{s} U_{pw} \frac{dU_{pw}}{ds} ds - \int_{s_p}^{s} q_1(s) \frac{dk}{ds} ds,$$

$$PR = \frac{1}{(\delta_{2m} U_{pw}^2)_{s_0}} \int_{s_0}^{s} u_\tau^2 \, ds,$$

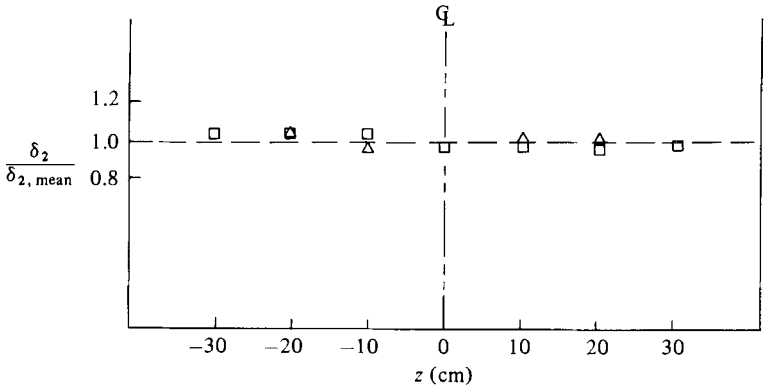

FIGURE 10. Spanwise distribution of momentum thickness at stations before and after the convex curvature: □, station 5; △, 13.

where

$$\delta_{2m} = \int_0^\infty (1+\kappa n)\frac{U(U_p-U)}{U_{pw}^2}\,dn,$$

$$q_1(s) = \int_0^\infty \frac{nU_p(U_p-U)}{U_{pw}^2}\,dn + \int_0^\infty \frac{nU(U_p-U)}{U_{pw}^2}\,dn,$$

and κ is the reciprocal of the wall radius of curvature.

The results of these calculations are shown in figure 9. Comparison with similar plots of two-dimensional experiments in Kline *et al.* (1968) shows that the flow was at least as two-dimensional as in other accepted experiments.

There is further evidence that the two-dimensionality of the flow was preserved. Figure 10 shows the spanwise distribution of momentum thickness measured in the recovery section, as well as the distribution upstream. It can be seen that the distribution is as flat in the recovery region as before the curvature. Previous experience (see Gillis *et al.* 1980) shows that even slight secondary flows cause the off-centreline values of δ_2 to increase much faster than the values in the centreline.

Comparison of data between the present experiment and the earlier experiment of Gillis & Johnston (1980) shows that such secondary flows do not significantly affect any turbulence or skin-friction data, although entrainment and momentum thickness data can be affected, if secondary flows are much larger than in the experiments reported here.

Because the flow in the recovery zone of this experiment was two-dimensional, the growth rate of boundary-layer mass flux could be used to estimate the entrainment rate. The rate of entrainment of free-stream fluid into a boundary layer is defined as the rate of growth of boundary-layer mass flux. For a flat, two-dimensional, incompressible boundary layer, the boundary layer mass flux per unit width is

$$I(s) = \rho U_\infty(\delta-\delta_1).$$

Over a curved wall, the situation is slightly more complicated. The basic definition of entrainment is, of course, the same. As shown in Gillis *et al.* (1980), the equivalent expression for a curved-wall boundary layer is

$$I(s) = U_{pw}\rho R \ln\frac{R+\delta}{R+\delta_1},$$

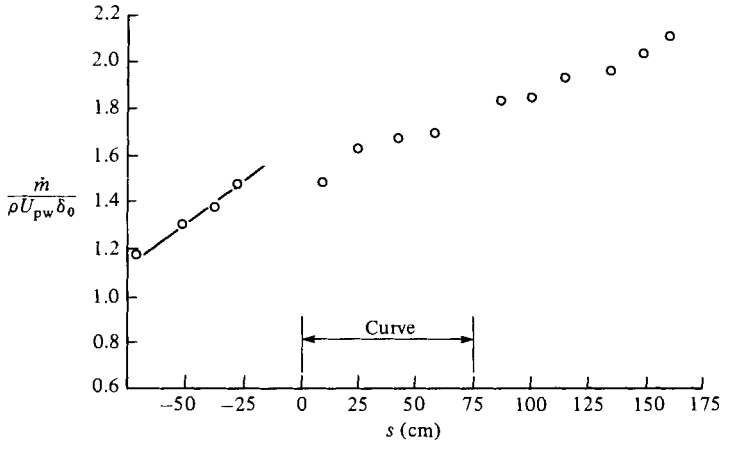

FIGURE 11. Growth of boundary-layer mass flux: ○, experiment; ——, calculated for flat wall.

where the displacement thickness is defined by

$$\int_0^{\delta} (U_p - U)\,\mathrm{d}n = \int_0^{\delta_1} U_p\,\mathrm{d}n.$$

It is clear from the plot (figure 11) that the entrainment rate is reduced by the curvature and remains low all the way through the recovery section. The solid line has the slope (entrainment rate) expected for a flat-plate boundary layer, and it fits the data upstream of the start of curvature.

2.2. *Turbulence data*

Figure 12 is an isometric plot of the shear-stress profiles at all 17 measuring stations in the case where $\delta_0/R \approx 0.1$. The first three profiles, at stations 3, 4 and 5, were taken upstream of curvature and are essentially the same as the profile taken by Klebanoff (1955) in a similar flow. The dots at $n/\delta = 0$ are the wall-shear values computed from the law of the wall. It can be seen that there is good agreement everywhere except at station 7. The profile at station 6 was taken exactly at the start of curvature and is similar to the profiles upstream. The profile at station 7, however, taken after only 13° of turning, shows the drastic effects of curvature. In a distance of only 2.8 boundary-layer thicknesses, the shear stress in the outer 70 % of the boundary layer has disappeared entirely. Profiles 7–10 in the curved region all have similar shapes, with a nearly linearly descending dropoff away from the wall. In the recovery region, the profile shape near the wall shows the positive slope deduced from the mean-velocity profiles as it slowly changes back to a zero slope with τ^+ equal to unity. The overshoot of $-\overline{u'v'}$ and wide region of high shear stress out to $n/\delta \approx 0.3$ for the profiles in the recovery region clearly shows the slowness of recovery.

Figure 2, in which the four profiles immediately upstream and downstream of the start of curvature have been plotted, shows how rapidly the effects of curvature appear. The profile at station 7 shows that the turbulent shear stress is negative (a result larger in magnitude than the uncertainty in the data in this region) over approximately the outer 60 % of the layer. The profile at station 8 shows a large region of negative shear stress. At station 9, the region of negative shear stress has become

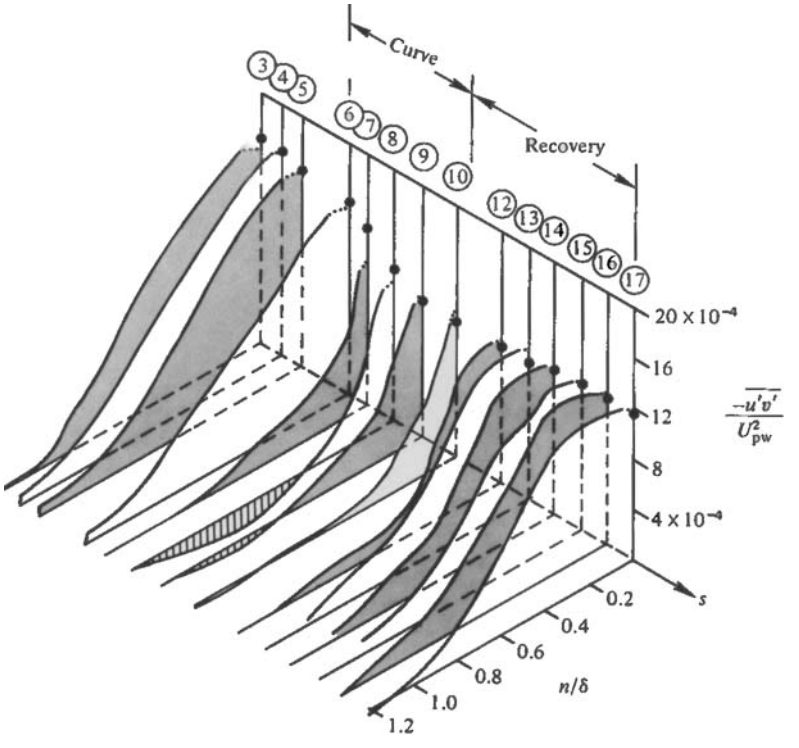

FIGURE 12. Isometric plot of shear-stress profiles as distance in flow direction: ●, wall skin friction calculated by Clauser plot.

smaller, and none of the profiles downstream shows any negative shear stress. There is no physical reason why the correlation of u' and v' should always be negative (producing a positive shear stress) when the velocity gradient is positive. The profile at station 9 shows that the magnitude of the negative shear stress has declined, and at station 10 in figure 12 there are no more regions of negative shear stress.

The reason for the appearance of negative shear stress in the curved boundary layer was given in a separate analysis of the present data by S. Honami (1980 private communication). For a flow over a curved surface, the Reynolds-stress transport equation can be written

$$\begin{aligned}\frac{\mathrm{D}(\overline{u'v'})}{\mathrm{D}t} = {} & \overline{u'^2}\left[\frac{\partial V}{\partial s} - \frac{U}{R}\right] + \left(1+\frac{n}{R}\right)\overline{v'^2}\frac{\partial U}{\partial n} - \frac{U}{R}(\overline{u'^2}-\overline{v'^2}) \\ & - \frac{p'}{\bar{\rho}}\left[\frac{\partial v'}{\partial s} + \left(1+\frac{n}{R}\right)\frac{\partial U}{\partial n}\right] \\ & + \frac{\partial}{\partial s}\left[\overline{\frac{p'v'}{\rho}} - \overline{u'^2v'}\right] + \left(1+\frac{n}{R}\right)\frac{\partial}{\partial n}\left[\overline{\frac{p'u'}{\rho}} + \overline{uv^2} + \frac{(\overline{2u'v'^2}-\overline{u'^3})}{R}\right] \\ & - \epsilon.\end{aligned}$$

The terms on the right-hand side have been grouped according to function. On the first line are the production terms. The second line is the pressure–strain term, which tends to change the orientation of the turbulent motions. On the third line are the

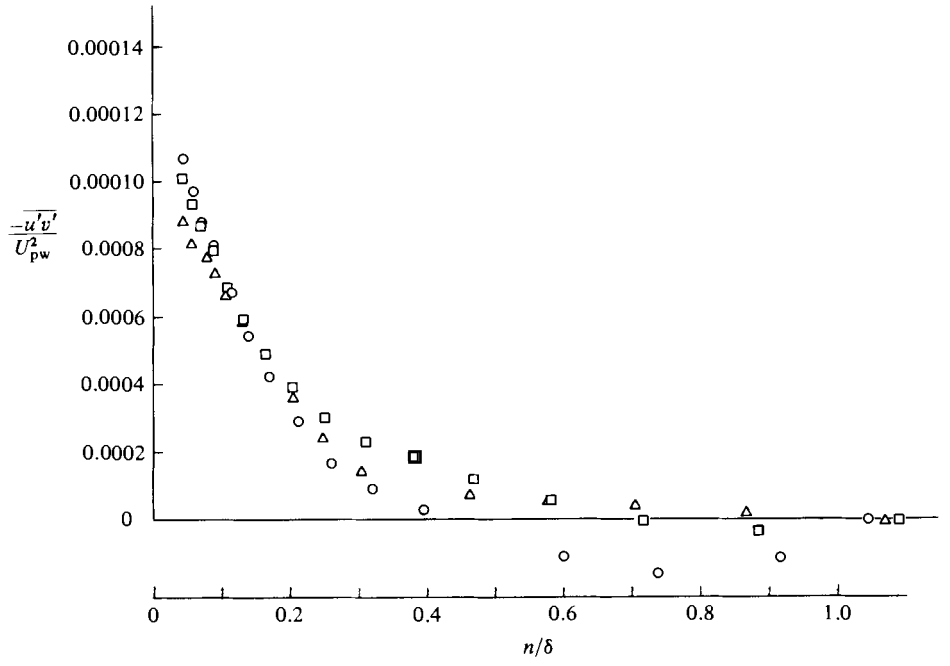

FIGURE 13. Collapse of inner-layer shear-stress profiles in curved region: ○, station 8; □, 9; △, 10.

diffusion terms, and the last line is the dissipation term. Over a curved wall the dominant production terms are

$$P = \overline{v'^2}\frac{\partial U}{\partial n} - (\overline{2u'^2} - \overline{v'^2})\frac{U}{R}.$$

For a flat wall, of course, only the first of the terms on the right-hand side is non-zero. The second term in the equation above appears suddenly at the start of curvature, and it tends to decrease the total production rate, since usually $2\overline{u'^2}$ is greater than $\overline{v'^2}$.

Calculations made with measured values of $\overline{u'^2}$ and $\overline{v'^2}$ from stations 5 and 7 show that, for a flat-wall profile like station 6, the production is positive at all values of n. For the curved-wall boundary layer, the total production is positive in the inner layer, but in the outer layers, the positive and negative production terms are about equal. This is the reason for the huge change in the outer-layer levels of $-\overline{u'v'}$ near the start of curvature. The negative production balances the positive production, and the dissipation reduces the shear-stress level to low values.

Figure 13 is a plot of the shear-stress profiles taken in the curved region. The sharp linear dropoff near the wall is clear. It is also clear that, in contrast with the rapid change at the start of curvature, the profiles do not change substantially as the flow moves downstream. Near the wall, the shear-stress profiles nearly collapse on each other when $\overline{u'v'}/u_\tau^2$ is plotted *vs.* R/δ. This collapse is due only to the fact that δ does not change very much in the curved region. As figure 4 shows, the appropriate scaling length appears to be R rather than δ. The profiles seem to be in a nearly asymptotic state, at least for $n/\delta < 0.4$.

Figure 14 is a plot of a, the ratio of shear stress to turbulent kinetic energy at three

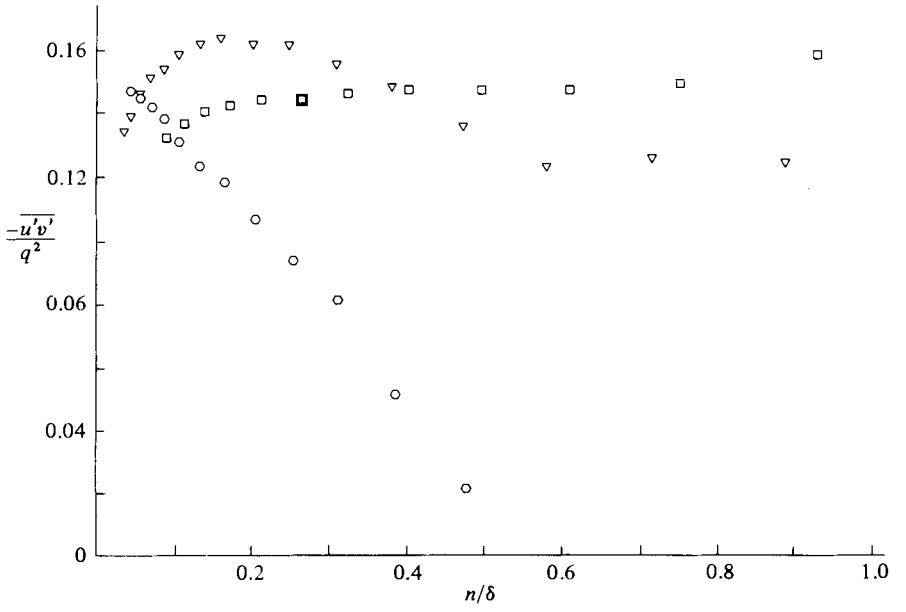

FIGURE 14. Structural parameter profiles for representative flat, curved and recovery stations: □, station 5 (upstream); ○, 9; ▽, 12 (first recovery).

typical stations. Upstream of curvature, a is nearly constant over almost all of the boundary layer and is about equal to 0.145, a value in good agreement with the previous flat-plate measurements of Klebanoff (1955). For the curved boundary layer, however, a becomes a strong function of position across the layer. Values of a beyond $n/\delta = 0.4$ are not very reliable, because of the uncertainty in $-\overline{u'v'}$ and q^2, both of which have low magnitudes. Many calculation methods employ the assumption that $-\overline{u'v'}/q^2$ is a constant, so it is clear that some modification will be necessary if these models are ever to handle curvature. In the recovery region, a very surprising trend is noticed. The recovery of the structural coefficient is very quick (compared with the sluggish recovery of the $-\overline{u'v'}$ and $\overline{u'^2}$ profiles).

In this experiment, separate measurements were taken of all the components of the two-dimensional Reynolds stress tensor. Comparison of the data showed that, for profiles taken in the curved region, the turbulence beyond $n/\delta \geqslant 0.35$ (where the shear stress was small) the measured values of the normal stresses were very close, and the turbulence was nearly isotropic. To show this, consider the scalar $b^2 = b_{ij}\,b_{ij}$ of a tensor which measures the anisotropy of turbulence. This anisotropy tensor, often used in turbulence models, is

$$b_{ij} = \frac{R_{ij} - \frac{1}{3}q^2\delta_{ij}}{q^2},$$

where R_{ij} is the Reynolds stress tensor. Figure 15 shows how the value of b^2 is affected by curvature at several stations in the boundary layer. Because of the growth of the boundary layer is small in the curved region, plotting b^2 along constant values of n/δ is almost the same as plotting b^2 along mean streamlines. At $y/\delta = 0.55$, the nearly isotropic nature of the outer-layer turbulence in the curve is clear; but the near wall, at $y/\delta = 0.10$, this is not true, but anisotropy seems to increase with distance in the curved region. Note, finally, that anisotropy recovers rapidly downstream of the curved region.

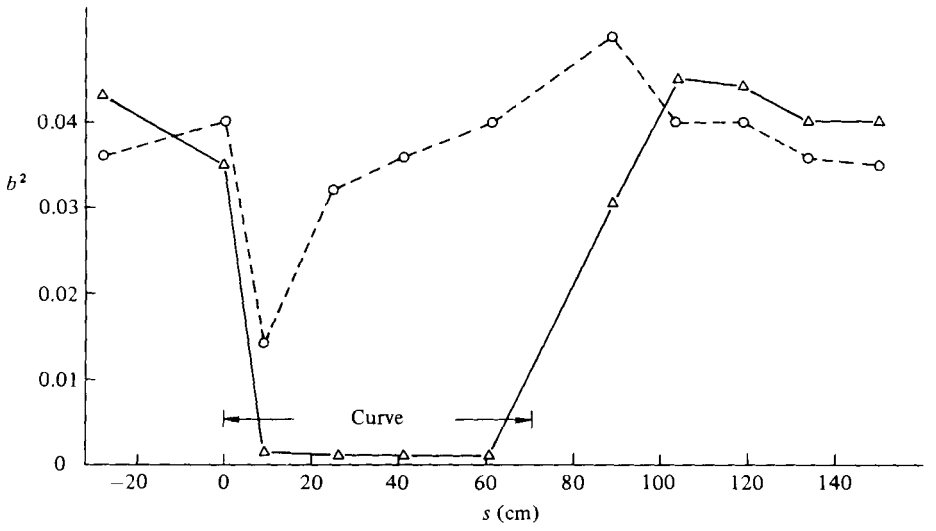

FIGURE 15. Plot of the anisotropy scalar b^2 *vs.* s, at two values of n/δ. ○, $n/\delta = 0.10$, inner layer; △, $n/\delta = 0.55$, outer layer.

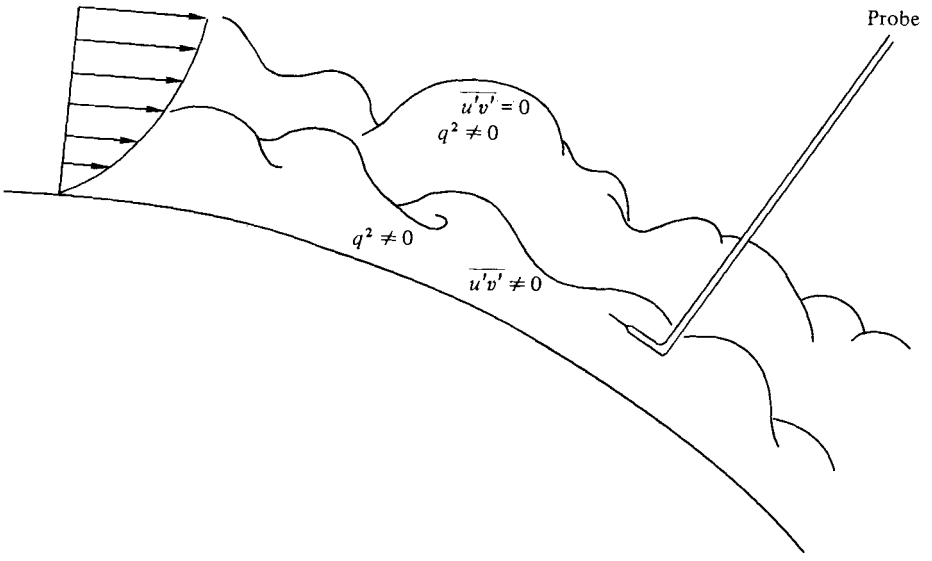

FIGURE 16. Two-layer conceptualization of the outer part of a curved boundary layer.

The shape of the turbulence profiles, the unusual behaviour of the structural coefficient, and the near-isotropy of the outer layer in the curved region suggest a possible physical interpretation for the data presented so far. As argued in §1, the main effect of the curvature is to reduce the scale of the turbulence. In the shear-stress profiles, the width of the active shear-stress layer has been drastically reduced to $\frac{1}{3}\delta$. The velocity gradient boundary layer, however, extends to δ. Thus, there is a two-layer structure in the outer layers of the curved and recovery region. Very near the wall there is normal turbulence with the usual value of structural coefficient. In the outer layer there is decaying, nearly isotropic 'debris' from the thick, turbulent boundary

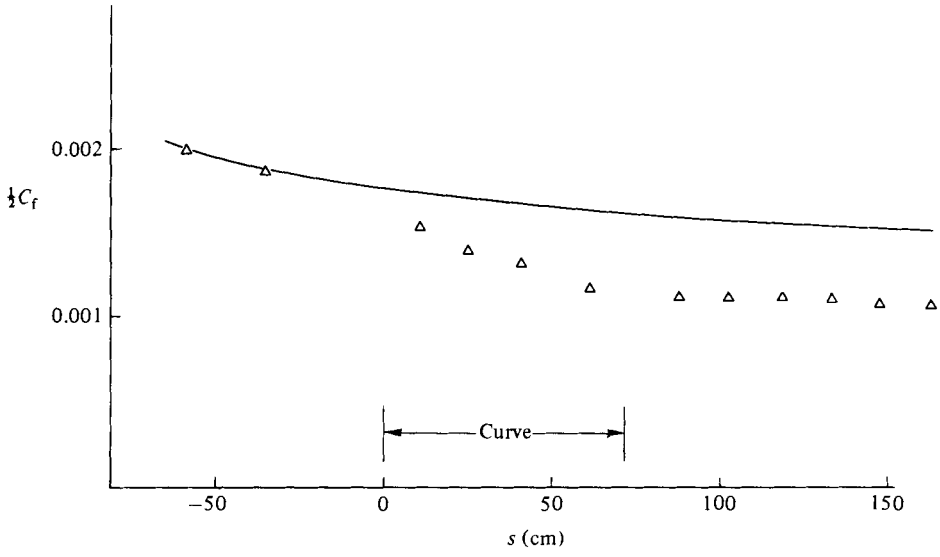

FIGURE 17. Skin friction (from mean-velocity profiles) *vs.* distance in the flow direction: △, data; ——, predicted friction for the same initial boundary layer on a flat wall.

layer upstream of curvature. This 'debris' is cut off from the direct Reynolds-stress-generating mechanisms of the wall and decays as it is convected downstream.

The idea that the 'turbulent shear layer' is concentrated in a narrower zone within the 'velocity-gradient layer' could also provide an explanation for the shape of the $-\overline{u'v'}/q^2$ profiles, if the 'turbulent shear layer' has its own intermittency, as sketched in figure 16. Assuming that the ratio of $-\overline{u'v'}/q^2$ in the 'turbulent shear layer' is about 0.145, as usual (and as it is near the wall), then a probe which time-averages $-\overline{u'v'}/q^2$ at a point where instantaneous $-\overline{u'v'}/q^2$ is fluctuating alternately between 0.145 (wall layer) and 0.0 (outer, decaying layer) could easily produce a profile like that at station 5 in figure 14.

Another experiment was run on the long-recovery rig. One of the upstream trips was removed and the remaining trip readjusted in order to give a ratio of boundary-layer thickness to radius of curvature of 0.05. This procedure enabled us to observe the effects of curvature at an intermediate value of δ_0/R. It was also supposed when we set up this experiment that the recovery process would be more complete, since the number of (velocity-gradient) boundary-layer thicknesses downstream of curvature was greater.

The skin-friction distribution for this case is plotted in figure 17, along with the flat-wall prediction. Despite the fact that the original boundary layer is only about one-half as thick as for the previous cases, the $\frac{1}{2}C_f$ curve is remarkably similar. The recovery after curvature appears to be no more advanced at the end of the recovery plate than in the experiment at $\delta_0/R \approx 0.10$.

One of the consequences of thinning the test surface layer was to increase problems with secondary flows generated on the endwalls. Since the boundary layers on the sidewalls were unaffected by the change from thick to thin test-surface boundary layer, the amount of secondary flow field coming off the side walls was the same as for the other experiment, where $\delta_0/R = 0.10$. The test-surface boundary-layer mass flux, however, was much less, and consequently the effects of the secondary flow are greater. Figure 18 shows *PL* and *PR* calculations for this experiment. The

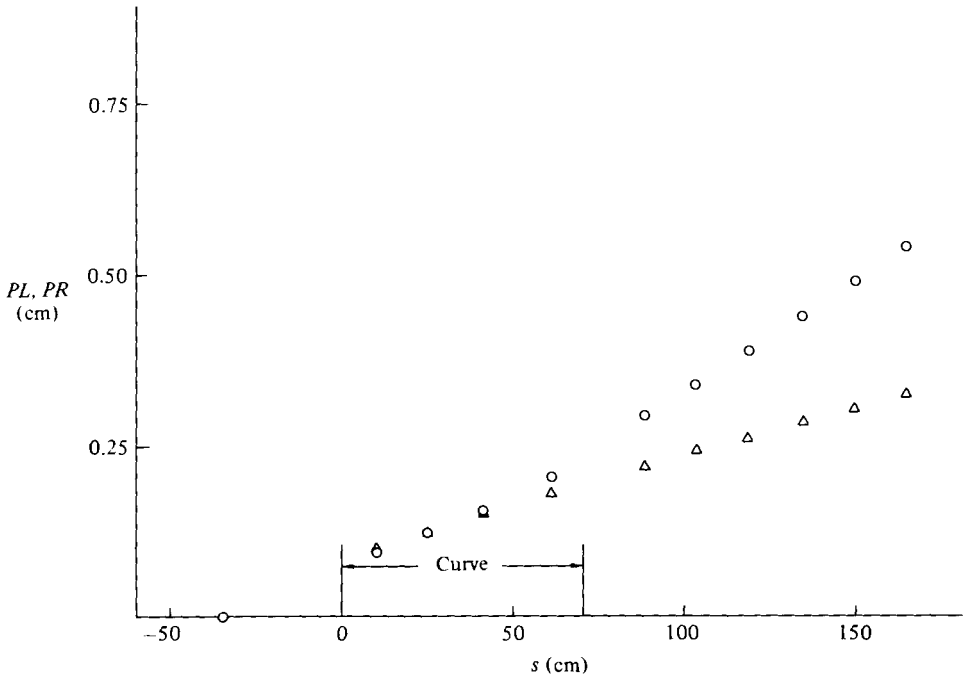

FIGURE 18. *PL* and *PR vs.* distance in the flow direction for the experiment at $\delta/R = 0.05$: ○, *PL*; △, *PR*.

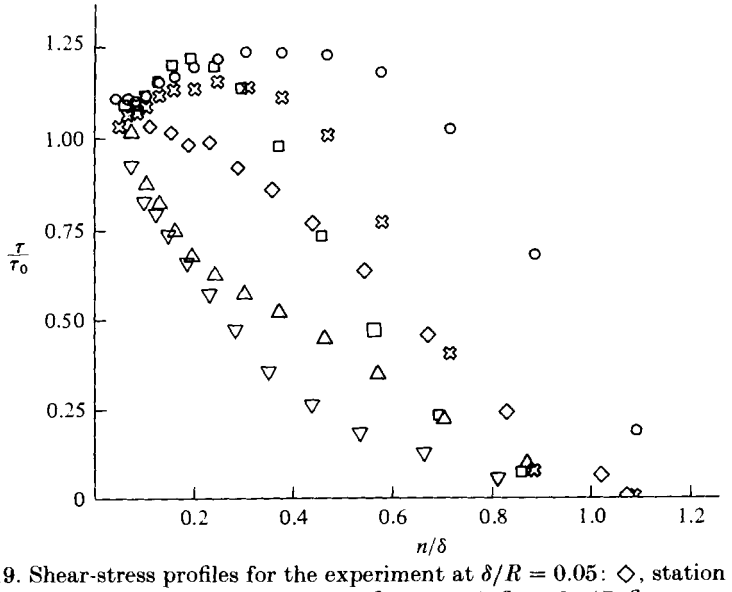

FIGURE 19. Shear-stress profiles for the experiment at $\delta/R = 0.05$: ◇, station 5; △, 7, curved; ▽, 9, curved; □, 12, flat; ⊠, 14, flat; ○, 17, flat.

secondary flows are clearly enough to influence the growth rate of integral parameters. Experience with the first experiment and that of Gillis & Johnston (1980) indicates that measurements of $\frac{1}{2}C_f$ and the turbulence quantities should not be greatly affected by secondary flows of this magnitude. However, it is probable that the secondary flows are responsible for the very small decrease in $\frac{1}{2}C_f$ in the recovery region of the $\delta/R \approx 0.05$ experiment. Without the secondary flows, there would

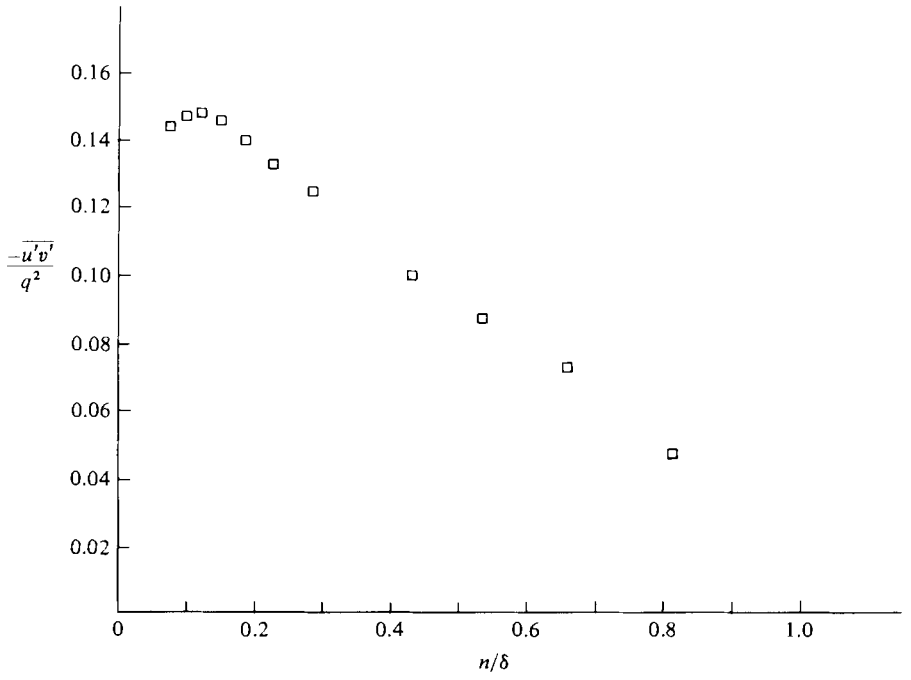

FIGURE 20. Plot of the structural coefficient for station 9 (after 78° of curvature) in the experiment at $\delta_0/R = 0.05$.

probably be some tendency for recovery of $\frac{1}{2}C_f$ in the $\delta_0/R \approx 0.05$ experiment, as there is in the $\delta_0/R = 0.10$ experiment.

Only six shear-stress profiles were taken in the last experiment. Measurements were made upstream; two profiles were located in the curved region and three were over the recovery plate. Figure 19 shows all these profiles.

The trends observed previously are reconfirmed here, except for a couple of peculiarities. First, in the profile taken near the end of curvature (station 9), the region over which there is appreciable shear stress extends over a greater fraction of δ than in the $\delta/R = 0.10$ cases. Secondly, in the last profile at station 17, the level of $-\overline{u'v'}/u_\tau^2$ beyond its maximum is much higher over the entire profile than for the measurements taken upstream. At $n/\delta \approx 0.50$, the value of $-\overline{u'v'}/u_\tau^2$ at station 17 is *twice* that at station 5.

As in the $\delta/R \approx 0.10$ experiments, the structural coefficient a became a function of position n/δ over the curved surface, as shown in figure 20. For this case, the steepness of the dropoff at large n/δ is much less than was the case at $\delta/R = 0.10$.

The data from both experiments, at $\delta/R = 0.10$ and at $\delta/R = 0.05$, show a striking degree of similarity downstream of the start of curvature. It is suggested that, as the width of the active shear layer is decreased, the large eddies which carry the 'history' of the turbulence structure are either destroyed or modified in such a way that the 'history' is lost. Downstream of the start of curvature, the initial conditions are largely irrelevant. Note that, in both flows we have examined, the initial boundary-layer thickness was larger than the thickness of the shear-stress-carrying region. The present suggestion may not be valid for layers that are very thin at the start of curvature, e.g. the flow of Meroney & Bradshaw (1975) and Hoffman & Bradshaw (1980).

Support for this interpretation comes mostly from the shear-stress profiles and most

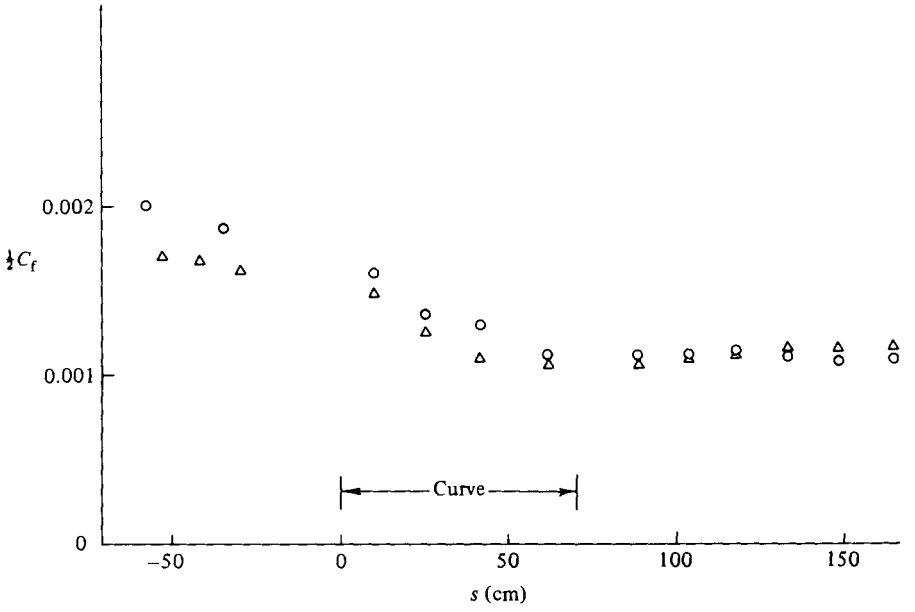

FIGURE 21. Comparison of skin-friction curves for $\delta_0/R = 0.10$ and $\delta_0/R = 0.05$: △, data, $\delta_0/R = 0.10$; ○, data, $\delta_0/R = 0.05$.

especially from figure 4, which shows the end-of-curvature profiles from the present two experiments together with profiles from an earlier, similar experiment and profile from So & Mellor in which the free-stream velocity and radius of curvature were somewhat different ($R = 32.56$ cm, $U_{pw} = 2404$ cm/s) from our cases. The data are normalized on R rather than δ, and they follow the same curve, showing that the shear-stress profile is a function of n/R rather than n/δ. It is, at most, only a weak function of U_{pw}. This is surprising, since the cross boundary-layer pressure gradient U^2/R is a strong function of U_{pw}. The weak-curvature data of Hoffman & Bradshaw (1980) do not follow the other data, however. Smits *et al.* (1979) did not measure shear-stress profiles over their curved wall, so it was impossible to check for the collapse of their data as well. However, the first profile they measured in the recovery section shows that the shear stress is confined to the region $n/R < 0.043$, indicating that the shear-stress profiles in the curved section may have been quite close to the curve of figure 4.

In figure 21, the skin-friction curves for experiments 1 and 2 have been overlaid. It can be seen that the curvature exerts an 'organizing influence' – the values of skin friction after the start of curvature are much closer than they were over the preplate. Measurements of Stanton number for the same two experiments, taken by Simon and Moffat (figure 3) show the similarity of conditions after curvature even more clearly.

The main effect of strong curvature, then, is to impose a limit on the size of the largest eddies. If the initial large-eddy size is larger than this limit, eddies larger than the limit must either shrink or be destroyed. In the recovery region, the large-scale eddies grow back slowly, just as large eddies grow slowly in a developing boundary layer.

Apparently our experiments at $\delta_0/R = 0.05$ and $\delta_0/R = 0.10$ simply approach the same 'asymptotic convex boundary layer' from two slightly different initial conditions. Whether an initially thin layer such as that of Hoffman & Bradshaw ($\delta/R \approx 0.01$)

approaches this limit from below is an open question. If our results do indeed show an asymptotic state, the results of Hoffman & Bradshaw, as plotted on figure 4, must be well below that asymptotic state.

3. Implications of the present results for the calculation of curved boundary layers by mixing-length models

The most important characteristic of the experimental results just presented is that the response of the boundary layer to the introduction of convex curvature is markedly different from its response to the disappearance of curvature. Not only is this clear from the plots of skin friction (figure 1 and 17), but also from the shear-stress profiles (figures 11 and 19) and from the entrainment (figure 10). This asymmetry of response is consistent with the explanation that, when the curvature is strong ($\delta_0/R > 0.04$), the large-scale eddies are forced to a new scaling length – the radius of curvature.

For the strong-curvature cases presented, the effect of the extra scaling length is a decrease in the size of the largest eddies. This process can presumably occur either by the 'shrinking' of eddies too large to be compatible with the new scaling length or by the complete dispersal of those eddies. When this action takes place, the 'history' of the boundary layer is lost.

When the extra scaling length disappears at the end of curvature, the boundary-layer turbulence does not spring back to its original structure, because the memory of the upstream turbulence structure has been lost. Some information about the upstream history of the layer is present in the mean-velocity profile, but the velocity gradient is only indirectly coupled to the turbulence structure. Thus there is no strong driving force for recovery, but only a gentle tendency of the large scales to reappear over a long distance.

The turbulent layers nearest the wall do not appear to be directly affected by curvature. This is best shown in the mixing-length profiles computed from the mean-velocity and shear-stress profiles from §2. As shown in figure 22–25, the mixing lengths near the wall still follow the formula $l = kn$.† Away from the wall, however, the mixing length becomes a constant at a much lower value of n. This result makes sense, since, very near the wall, the wall will look flat to the small-scale turbulence. Another indication that curvature has its effect mainly on the large-scale eddies is the big (and immediate) change in the entrainment rate at the start of curvature.

Taken with other indications that the curvature effects are strongest in the wake region of the mean profile, it is obvious that simple turbulence models like the Prandtl mixing length will have trouble, because they are based on local conditions. The curvature effects act on the large scales, which are not immediately controlled by local conditions. In his mixing-length model, Bradshaw accounted for the upstream influence with a first-order lag equation to calculate an 'effective' radius of curvature. The lag equation he suggested,

$$\frac{\mathrm{d}(1/Re_{\mathrm{eff}})}{\mathrm{d}s} = \frac{1}{10\delta}\left[\frac{1}{R} - \frac{1}{Re_{\mathrm{eff}}}\right],$$

predicts a symmetric response – meaning that curvature effects should appear and disappear at the same rate. One possibility for modifying the above equation is to

† Later work by Adams & Johnston (1981) suggests a better fit $l/l_0 = 1/(1+\beta Ri)$, where $l_0 = kn$ and $Ri \approx 2U/(R\,\partial U/\partial n)$. Very near the wall, Ri is small because $\partial u/\partial n$ is very large. Thus $1/(1+\beta Ri) \approx 1$.

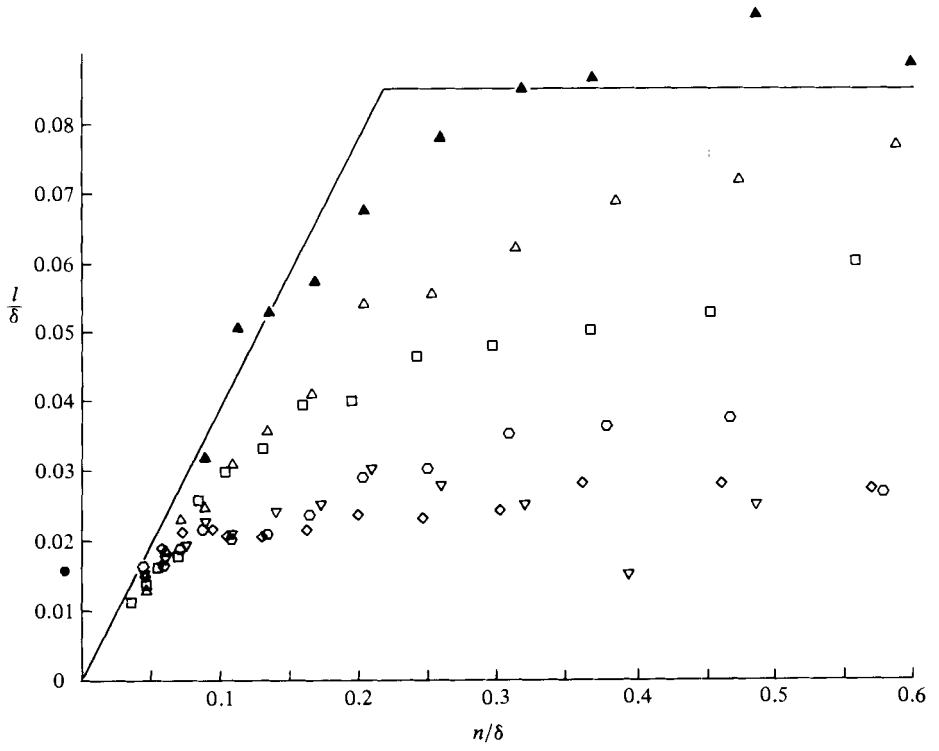

FIGURE 22. Curved-region mixing-length profiles for the experiment at $\delta_0/R = 0.10$; ▲, station 5, flat wall; △, 6, start of wall curvature; □, 7, after 12° of wall curvature; ▽, 8, after 32° of wall curvature; ○, 9, after 53° of wall curvature; ◇, 10, after 78° of wall curvature.

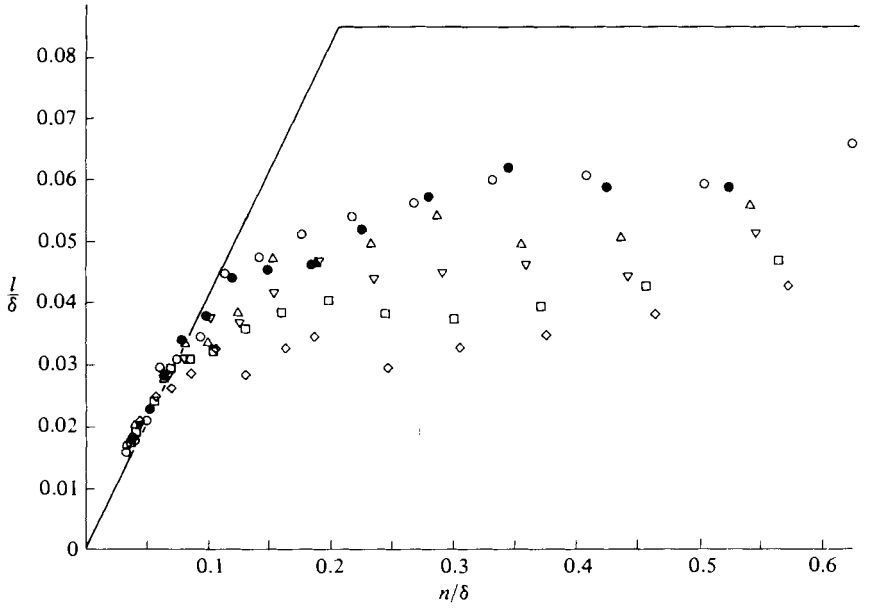

FIGURE 23. Recovery-region mixing-length profiles for the experiment at $\delta_0/R = 0.10$: ▽, station 12; □, 13; ▽, 14; △, 15; ●, 16; ○, 17.

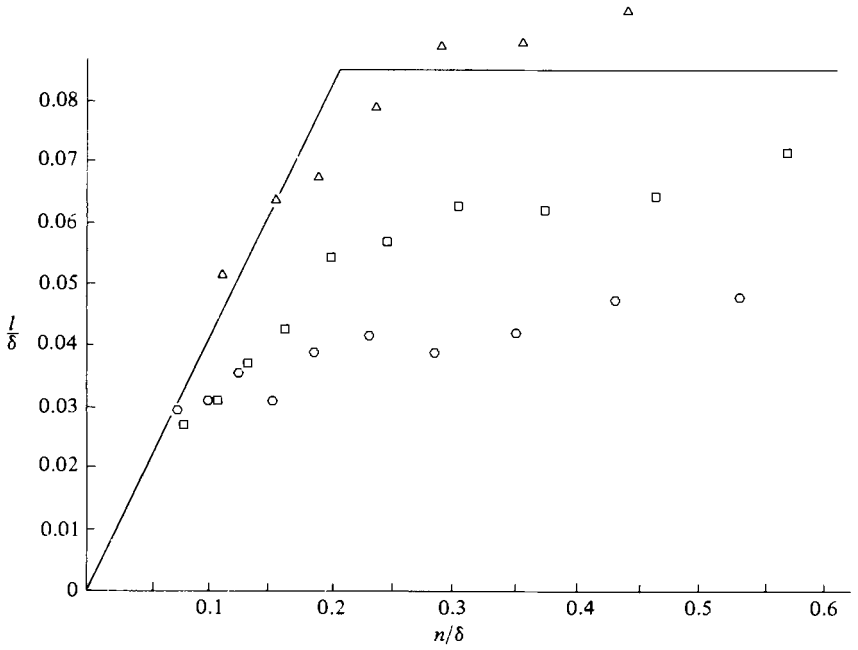

FIGURE 24. Curved-region mixing-length profiles for the experiment at $\delta_0/R = 0.05$: △, station 5, upstream of curvature; □, 7, after 12° of wall curvature; ○, 9, after 53° of wall curvature.

make the recovery-rate parameter ($1/10\delta$) a function of the amount of shear stress in the boundary layer. Experiments by the authors with such a model did indeed show improved fit to the data, but it could not easily be made to account for the great difference in the rate of appearance and disappearance of curvature effects.

The situation for mixing-length models is not all bad. The data show a relationship between the shear stress and the mean-velocity gradient which is consistent with the mixing-length model. During the curve, the mean-velocity gradient in the outer layer increases, because the shear stress is decreased. In the recovery region, this much-increased mean-velocity gradient can combine with an increasing mixing length to produce a maximum in the shear-stress profile away from the wall, as seen in the data. Also, the same combination of large outer-layer velocity gradients and an increasing mixing length will result in the overshoot of shear stress which is seen in the data near the end of the recovery section.

The fact that there is similarity in the shear-stress profiles and mixing lengths for both experiments, despite the factor-of-two difference in boundary-layer widths, implies that for asymptotic curvature the outer-layer mixing length is a function of the radius of curvature alone in the curved region. When inventing a mixing-length curvature model, the question arises – what is the proper scaling length at the end of the curvature? It is clear that simply switching back to scaling the mixing length based on the 99% velocity thickness will cause an almost immediate recovery. The lag equation approach is one way to simulate the slow recovery. However, all evidence in the curved region is that the turbulence structure has been disassociated from the upstream history of the boundary layer. Thus the appearance of δ in the lag equation seems inappropriate. For this reason, it seems more likely that there is some more appropriate scaling length within the boundary layer.

For boundary layers on flat surfaces in moderate pressure gradients, the method

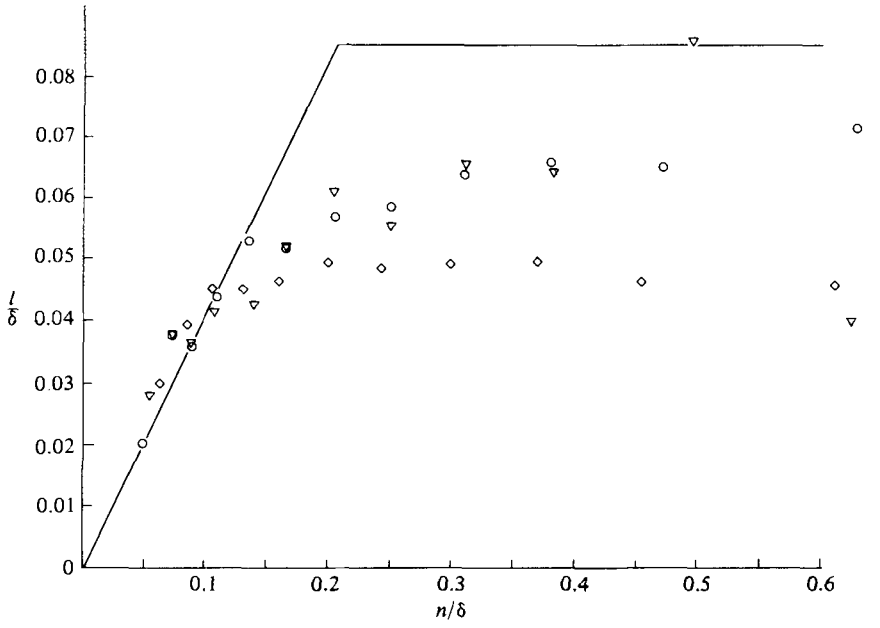

FIGURE 25. Recovery-region mixing-length profiles for the experiment at $\delta_0/R = 0.05$: ◇, station 12; ▽, 14; ○, 17.

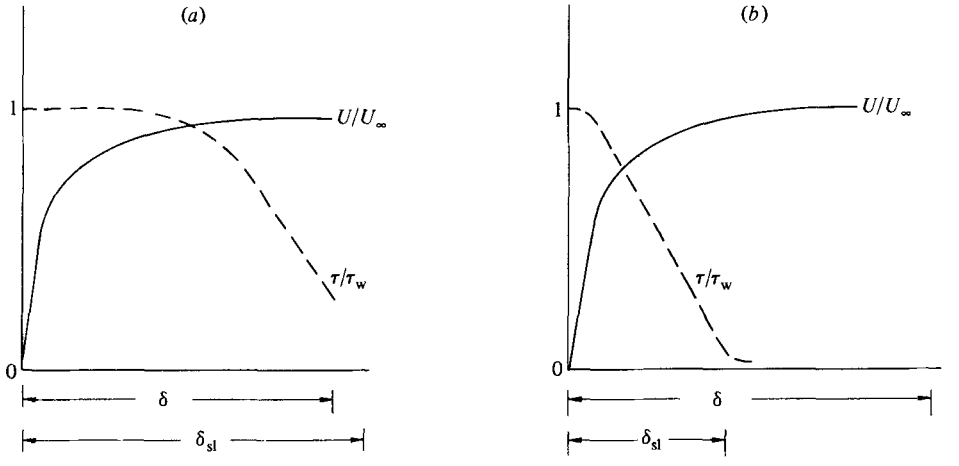

Figure 26. (*a*) Illustration of δ_{sl} on flat wall: ——, mean velocity; – – –, shear stress. (*b*) Illustration of δ_{sl} on curved wall: ——, mean velocity; – – –, shear stress.

of scaling the mixing length on δ has been successful. In the last section, it was argued that, when the turbulence structure adjusts to the radius of curvature as the dominant scaling length, it is compressed within the velocity gradient layer. One way to reflect this concept with a turbulence model would be to make the width of the active shear layer the scale for the mixing lengths in the outer region. This idea is illustrated in figure 26(*a*, *b*). The shear-layer width for a flat-plate boundary layer is approximately the same as the width of the velocity-gradient layer, but for a curved or recovering boundary layer they differ greatly.

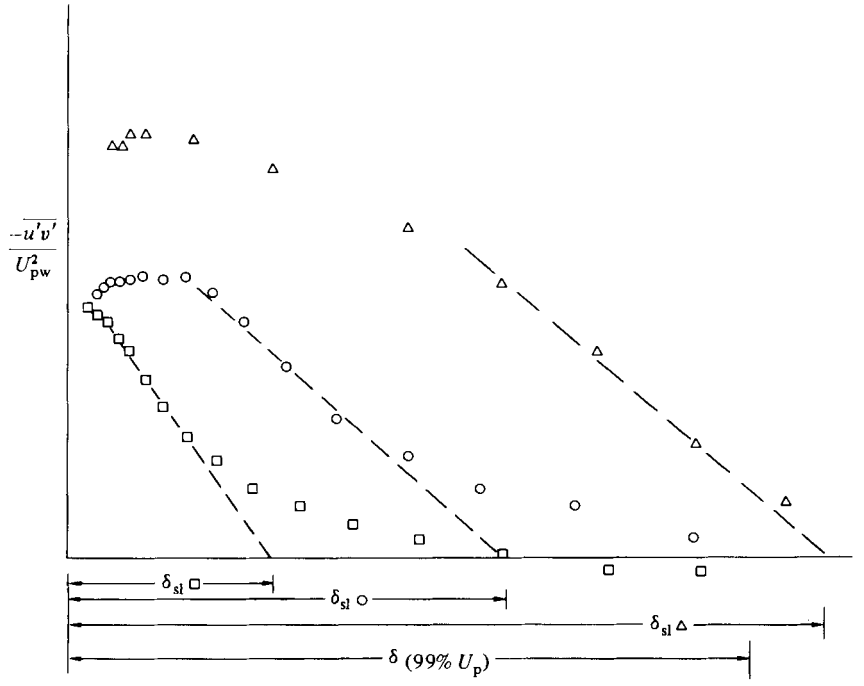

FIGURE 27. Method of determining δ_{sl} by extrapolating shear-stress profile: ---, extrapolation; △, data, flat wall; □, data, curved wall; ○, data, recovery from curvature.

A model based on this idea, in which the outer-layer mixing length is scaled on the shear-layer thickness and the near-wall mixing length is untouched or only changed slightly, could account for the slow recovery in a natural way without a lag equation. It also fits in with the physical observations of §2.

To test this idea, we have made the following non-rigorous calculations. First, the shear-layer width δ_{sl} was somewhat arbitrarily defined by extrapolating (by means of a straight-line fit by the method of least squares) the linear descending portion of the shear-stress curves, as shown in figure 27.

Next, we computed the average outer-layer mixing length. The outer layer was defined as the region outside the point where the mixing length differed significantly from kn but within δ_{sl}.

The results are shown in table 1. Naturally, these results can be informative only in a qualitative sense because of the arbitrary nature of the definitions above and the scatter of the data on which they are based. Nevertheless, they show that δ_{sl} could be a good scaling length, since the ratio of mixing length to δ_{sl} is approximately constant at 0.07 everywhere except at the start of curvature. One such model is discussed in Gillis *et al.* (1980). A simplified, practical version of this model was developed recently by Adams & Johnston (1981) which uses the wall radius R directly to scale l in the curved region, and a different lag model for recovery.

4. Conclusions

The principal conclusions of this work are as follows.

(i) The main effect of the introduction of surface curvature is a significant and immediate reduction in the turbulence lengthscale (as measured by the mixing

	Flat			Curved					Recovery					
Station	4	5	6	7	8	9	10	11	12	13	14	15	16	17
$l/\delta_{s1}, \frac{\delta}{R} \approx 0.10$	0.077	0.093		0.159	0.093	0.092	0.064		0.069	0.074	0.069	0.062	0.061	0.064
$l/\delta_{s1}, \frac{\delta}{R} \approx 0.05$	—	0.094		—	—	0.064	—		0.063	—	0.068	—	—	0.062
Distance from start of curvature (cm)	−41.3	−29.9	0.00	10.4	25.2	41.5	61.8		88.5	103.4	19.0	124.8	149.4	164.8

TABLE 1. Outer-layer mixing length divided by shear-layer width

length). Once this lengthscale is reduced, it regenerates very slowly, even if the boundary layer is flowing over a flat surface downstream of a region of significant curvature.

The reduction of eddy lengthscale caused by the curvature, through the action of the normal pressure gradient $\rho U^2/R$ is accompanied by a collapse of the active shear-stress layer to a thickness less than the thickness δ of the velocity-gradient boundary layer. The width of the velocity-gradient boundary layer is mainly determined by flow upstream of curvature; the width of the active shear layer is chiefly determined by local conditions in the curved region. Once the shear-stress layer has collapsed, it can regrow only at the rate characteristic of a thinner developing boundary layer. This rate is slow enough to account for the slow redevelopment of the shear-stress layer, after curvature, on the flat recovery surface.

After 'compression' of the shear-stress layer, the turbulence at large values of n/δ, beyond the shear-stress layer but within the velocity-gradient layer, is effectively isolated from the wall layers. It has little production, and consequently dissipation causes decay of the turbulent energy in the outer layers.

(ii) Shear-stress profiles taken in the curved regions for our two different sets of initial conditions ($\delta_0/R = 0.05$ and $\delta_0/R = 0.10$) and the data of So & Mellor (with different radius of curvature and free-stream velocity) collapse when $\overline{uv}/u_\tau^2$ is plotted against n/R. This behaviour indicates that, after the compression of the turbulent shear-stress layer, the large-scale eddies which carry the upstream history of the boundary layer are destroyed and the initial conditions no longer matter. The collapse of profile indicates that there may be an asymptotic shear-stress profile, at least for zero-pressure-gradient flow over convex surfaces with initial values of δ/R greater than $\frac{1}{20}$.

(iii) In the curved region, the law of the wall fits the data with the same constants used on the flat wall. The log region does not extend as far out in the boundary layer, ending near $y^+ = 100$. In addition, near the wall, the mixing length still scales a distance from the wall, as it does for no curvature. These observations indicate that the near-wall layers are not as strongly affected by the curvature as is the wake region.

(iv) It was found that, for this experiment, the outer-layer mixing length scaled on the width of the shear-stress layer rather than on the velocity-gradient-layer thickness δ.

This work was supported by grants NASA-NSG-3124 and NAG 3-3, administered by Dr Raymond E. Gaugler of the NASA-Lewis Research Center. We also acknowledge the advice of Professors R. J. Moffat and W. M. Kays, and the participation of Professor Terry Simon and Dr Russell Westphal. We are also grateful to Professor Shinji Honami for his assistance during his stay at Stanford. Finally the authors would like to thank the referees who reviewed this paper for the Journal; they made several helpful observations.

REFERENCES

ADAMS, E. & JOHNSTON, J. P. 1981 A mixing-length model for the prediction of convex curvature effects on turbulent boundary layers. *Rep.* IL-42, *Thermosci. Div., Mech. Engng Dept, Stanford.*

BRADSHAW, P. 1969 The analogy between streamline curvature and buoyancy in turbulent shear flow. *J. Fluid Mech.* **36**, 177.

BRADSHAW, P. 1973 Effect of streamline curvature on turbulent flow. *AGARDograph* 169.

CASTRO, I. R. & BRADSHAW, P. 1976 The turbulence structure of a highly curved mixing layer. *J. Fluid Mech.* **73**, 265.

CEBECI, T., HIRSH, R. S. & WHITELAW, J. H. 1979 On the calculation of laminar and turbulent boundary layers on longitudinally curved surfaces. *AIAA J.* **17**, 434.

ESKINAZI, S. & YEH, H. 1956 An investigation on fully developed turbulent flows in a curved channel. *J. Aero. Sci.* **23**, 23.

GIBSON, M. M., JONES, W. P. & YOUNIS, B. A. 1980 Calculation of turbulent boundary layers on curved surfaces, *Mech. Engng Dept, Imperial College, Rep.* FS/80/6.

GILLIS, J. C. & JOHNSTON, J. P. 1980 Experiments on the turbulent boundary layer over convex walls, and its recovery to flat-wall conditions. In *Selected Papers from the 2nd Intl Symp. on Turbulent Shear Flows*. Springer.

GILLIS, J. C., JOHNSTON, J. P., MOFFAT, R. J. & KAYS, W. M. 1980 *Rep.* HMT-31, *Stanford University Dept Mech. Engng.*

HOFFMANN, P. H. & BRADSHAW, P. 1978 Turbulent boundary layers on surfaces of mild longitudinal curvature. *Imperial College Aero Rep.* 78–04.

IRWIN, H. P. A. H. & SMITH, P. A. 1975 Prediction of the effect of streamline curvature on turbulence. *Phys. Fluids* **18**, 624.

JOHNSTON, J. P. & EIDE, S. A. 1976 Turbulent boundary layers in centrifugal compressor blades: prediction of the effects of surface curvature and rotation. *Trans. ASME* I: *J. Fluids Engng* **98**, 374.

JONES, W. P. & LAUNDER, B. E. 1972 The calculation of low Reynolds number phenomena with a two-equation model of turbulence. *Intl J. Heat Mass Transfer.* **15**, 301.

KÁRMÁN, T. VON 1934 Some aspects of the turbulence problem. In *Proc. 4th Intl Congr. Appl. Mech., Cambridge*, p. 54.

KLEBANOFF, P. S. 1955 Characteristics of turbulence in a boundary layer with zero pressure gradient. *NACA Rep.* 1247.

KLINE, S. J. *et al.* 1969 In *Proc. 1968 AFOSR–IFP–Stanford Conf. on the Computation of Turbulent Boundary Layers, Stanford University.*

LAUNDER, B. E., PRIDDIN, C. H. & SHARMA, B. I. 1977 The calculation of turbulent boundary layers on spinning and curved surfaces. *Trans. ASME* I: *J. Fluids Engng.* **99**, 231.

LAUNDER, B. E., REESE, G. J. &RODI, W. 1975 Progress in the development of a Reynolds-stress turbulence closure. *J. Fluid Mech.* **68**, 537.

MERONEY, R. N. & BRADSHAW, P. 1975 Turbulent boundary layer growth over a longitudinally curved surface. *AIAA J.* **13**, 1448.

PATEL, V. C. 1968 The effects of curvature on the turbulent boundary layer. *Aero. Res. Counc.* ARC 30427, FM 3974.

RAMAPRIAN, B. S. & SHIVAPRASHAD, B. G. 1978 The structure of turbulent boundary layers along mildly curved surfaces. *J. Fluid Mech.* **85**, 273.

RASTOGI, A. K. & WHITELAW, J. H. 1971 Procedure for predicting the influence of longitudinal surface curvature on boundary layer flow. *ASME* 71-WA/FE-37.

RAYLEIGH, LORD 1917 On the dynamics of revolving fluids. *Proc. R. Soc. Lond.* **A93**, 148.

SCHMIDBAUER, H. 1936 Behavior of turbulent boundary layers in curved convex walls. *NACA* TM 791.

SIMON, T. W. *et al.* 1981 Turbulent boundary layer heat transfer experiments: convex curvature effects, including introduction and recovery. *Rep.* HMT-31, *Thermosci. Div., Dept Mech. Engng, Stanford.*

SIMON, T. W. & HONAMI, S. 1981 Incompressible flow entry cases having boundary layers with streamwise wall curvature (0230). *Final Evaluation Report for the* 1980–81 *AFOSR–HTTM–Stanford Conf. on Complex Turbulent Flows: Comparison of Computation and Experiment, Thermosci. Div., Mech. Engng Dept, Stanford.*

SMITS, A. J., YOUNG, S. T. B. & BRADSHAW, P. 1979 The effects of short regions of high surface curvature on turbulent boundary layers. *J. Fluid Mech.* **94**, 243.

SO, R. M. S. 1978 Turbulent boundary layers with large streamline curvature effects. *Z. angew. Math. Phys.* **29**, 55.

SO, R. M. C. & MELLOR, G. L. 1972 An experimental investigation of turbulent boundary layers along curved surfaces. *NASA*-CR-1940.

So, R. M. C. & Mellor, G. L. 1973 Experiment on convex curvature effects in turbulent boundary layers. *J. Fluid Mech.* **60**, 43.

Thomann, H. 1967 Effect of streamwise wall curvature on heat transfer in a turbulent boundary layer. *J. Fluid Mech.* **33**, 283.

Wattendorf, F. L. 1935 A study of the effect of curvature on fully developed turbulent flow. *Proc. R. Soc. Lond.* **148**, 565.

Wendt, F. 1953 Turbulente Strömungen zwischen zwei rotierenden conaxialen Zylindren. *Ing.-Arch* **4**, 577.

Wilcken, H. 1967 Effects of curved surfaces on turbulent boundary layers. *NASA* TTF 11421.